



Microstructure and thermoelectric properties of screen-printed thick-films of misfit-layered cobalt oxides with Ag addition

Van Nong, Ngo; Samson, Alfred Junio; Pryds, Nini; Linderorth, Søren

Published in:
Journal of Electronic Materials

Link to article, DOI:
[10.1007/s11664-011-1848-x](https://doi.org/10.1007/s11664-011-1848-x)

Publication date:
2012

[Link back to DTU Orbit](#)

Citation (APA):
Van Nong, N., Samson, A. J., Pryds, N., & Linderorth, S. (2012). Microstructure and thermoelectric properties of screen-printed thick-films of misfit-layered cobalt oxides with Ag addition. *Journal of Electronic Materials*, 41(6), 1280-1285. <https://doi.org/10.1007/s11664-011-1848-x>

General rights

Copyright and moral rights for the publications made accessible in the public portal are retained by the authors and/or other copyright owners and it is a condition of accessing publications that users recognise and abide by the legal requirements associated with these rights.

- Users may download and print one copy of any publication from the public portal for the purpose of private study or research.
- You may not further distribute the material or use it for any profit-making activity or commercial gain
- You may freely distribute the URL identifying the publication in the public portal

If you believe that this document breaches copyright please contact us providing details, and we will remove access to the work immediately and investigate your claim.

Microstructure and thermoelectric properties of screen-printed thick-films of misfit-layered cobalt oxides with Ag addition

NGO VAN NONG¹, ALFRED JUNIO SAMSON, NINI PRYDS and SØREN LINDEROTH

Fuel Cells and Solid State Chemistry Division, Risø National Laboratory for Sustainable Energy, Technical University of Denmark, 4000 Roskilde, Denmark.

¹–e-mail: ngno@risoe.dtu.dk.

Abstract

Thermoelectric properties of thick-films (~60 μm), which were prepared by a screen printing technique using *p*-type misfit-layered cobalt oxide $\text{Ca}_3\text{Co}_4\text{O}_{9+\delta}$ with Ag addition, have been studied. The screen-printed films were sintered in air at various temperatures ranging from 973 K to 1223 K. After each sintering process, crystal and microstructure analyses were carried out in order to determine an optimal sintering condition. The results show that thermoelectric properties of pure $\text{Ca}_3\text{Co}_4\text{O}_{9+\delta}$ thick-film are comparable with cold-isostatic-pressed (CIP) samples. We found that the maximum power factor was improved about 67% (0.3 mW/mK^2) for a film with proper silver (Ag) metallic inclusions as compared to 0.18 mW/mK^2 for the film of pure $\text{Ca}_3\text{Co}_4\text{O}_{9+\delta}$ under the same sintering condition at 1223 K for 2 h in air.

Keywords: *Misfit-layered cobaltite, thermoelectric oxide, power factor, nanoinclusion*

INTRODUCTION

Thermoelectric generators, which convert heat directly into electricity in the presence of a temperature difference, provide a promising solution to the global challenges of finding new reliable, cleaner, and more environmentally friendly sources of energy.¹⁻³ These devices have the potential to increase the utilization of industrial or home waste heat by recapturing a portion of the waste heat from these sources and generating electricity.² At present, device conversion efficiencies are low (~5%)³, compared to other power generators from solar energy or another heat source¹, and more importantly their manufacturing process using bulk thermoelectric elements is expensive and time consuming. Another problem is the difficulty in scaling up to mass-production by the conventional processing.

Screen-printing technology has been demonstrated as a cost-effective and simple method, which is suitable for mass-production of thermoelectric modules.⁴⁻⁶ An advantage of this technology is that it allows to control the dimensional factor, referring to the thickness (or length) of the thermoelectric elements.⁴ When the thickness of thermoelectric materials is reduced, the maximum amount of heat that can be pumped as the temperature difference between hot and cold sides substantially increases resulting from a high heat flux and low thermal resistance along the thin-direction.

In this work, we have employed a printing technique to prepare *p*-type thermoelectric thick-films using misfit-layered cobaltite-based materials, which have been intensively investigated because of their good thermoelectric performance and their highly thermal and chemical stabilities even up to 1200 K in air.⁷⁻¹⁶ Thick-films of pure $\text{Ca}_3\text{Co}_4\text{O}_{9+\delta}$ material were fabricated and sintered at various temperatures ranging from 973 K up to 1223 K. Their microstructure and thermoelectric properties were investigated in order to determine an optimum sintering condition. Further investigations were focused on thick-films of $\text{Ca}_3\text{Co}_4\text{O}_{9+\delta}$ with various levels of Ag addition. A thick-film with a proper amount of Ag inclusions was found to exhibit a maximum power factor of $\sim 0.3 \text{ mW/mK}^2$, which is about 67% higher than a similar pure screen-printed $\text{Ca}_3\text{Co}_4\text{O}_{9+\delta}$ under the same sintering conditions at 1223 K for 2 h in air.

EXPERIMENTAL PROCEDURES

Polycrystalline **powder** samples of $\text{Ca}_{3-x}\text{Ag}_x\text{Co}_4\text{O}_{9+\delta}$ ($x = 0, 0.05, 0.1, \text{ and } 0.15$) were synthesized by solid-state reaction. The appropriate amounts of CaCO_3 (99.5%), Co_3O_4 (99.7%) powders and AgNO_3 (99.99%) solution were mixed by ball milling with ethanol for **36** h. The resulting mixture was dried and calcined at 1223 K for 24 h in air. $\text{Ca}_{3-x}\text{Ag}_x\text{Co}_4\text{O}_{9+\delta}$ inks, consisting of powder-dispersant-binder mixture were prepared and screen printed onto a $5 \times 5 \text{ cm}^2$, dense $290 \mu\text{m}$ thick $\text{Ce}_{0.9}\text{Gd}_{0.1}\text{O}_{1.95}$ (CGO) substrate (KERAFL). The screen printed samples were then sintered at 973 K, 1123 K, 1173 K and 1223 K in air for 1-2 h in order to determine an optimum sintering condition. For comparison, the powders after calcining at 1223 K in air for 24 h were pressed using cold-isostatic-**pressed** (CIP) technique under a pressure of 250 MPa during 1 min. CIP-samples were then further sintered at 1223 K in air for another 24 h.

The phase purity of the powders and the deposited layers on dense CGO substrate was checked by the X-ray diffraction (XRD) on a BrukerD8 diffractometer with $\text{Cu K}\alpha$ radiation. The microstructures of the sintered thick-films were analyzed using a Zeiss Supra 35 scanning electron microscope (SEM) system. The **in-plane** electrical resistivity and thermoelectric power were measured simultaneously using an ULVAC-RIKO ZEM3 thermoelectric property measurement system in **-0.9 bar helium (purity 99.999% with < 0.5 ppm residual oxygen)**.

RESULTS AND DISCUSSION

Figure 1 displays powder XRD patterns of $\text{Ca}_{3-x}\text{Ag}_x\text{Co}_4\text{O}_{9+\delta}$ ($x = 0, x = 0.05, x = 0.10, \text{ and } x = 0.15$), showing that most of the diffraction peaks are identical to the $\text{Ca}_3\text{Co}_4\text{O}_{9+\delta}$ phase with the JCPDS card (PDF #21-0139). Two additional XRD peaks at $2\theta \approx 38.1^\circ$ and 44.3° were found to fit well with two the strongest peaks of Ag (PDF# 01-1167), which could also be observed even for composition with low Ag concentration such as $x = 0.05$. In addition, the intensity of these peaks increased with increasing Ag concentration, indicating that these peaks indeed belong to the metallic Ag. The existence of excess Ag suggests that silver most likely agglomerated as inclusions at grains boundaries or dispersed in the grains interior instead of doping at the Ca-site. XRD analysis of the print-screened layers after sintering also revealed that the films are pure phase of $\text{Ca}_3\text{Co}_4\text{O}_{9+\delta}$ with similar traces of metallic Ag.

Figure 2a-d shows SEM images for the fractured surfaces of pure sintered films $\text{Ca}_3\text{Co}_4\text{O}_{9+\delta}$ at 793 K - 1 h, 1123 K - 1 h, 1173 K - 2 h, and 1223 K - 2 h, respectively. It is clear from Fig. 2 that the morphology of the films changed when the sintering temperature was increased from 973 K, 1123 K, and 1173 K to 1223 K. For the film, which was sintered at 973 K for 1 h, the morphology looks as if the grains have just started sintering, i.e. many small grains surround the large ones, which are separated and poorly faceted (Fig. 2a). Moreover, it appears as if the adhesion between the substrate and the film is very poor, e.g. as illustrated by the air-gaps (Fig. 2a). With increasing sintering temperature e.g. to 1123 K - 1 h, the grains started growing and forming a plate-like morphology (Fig. 2b). The evolution of the microstructure became more pronounced with further increasing sintering temperature and time i.e. at 1173 K (Fig. 2c) and 1223 K for 2 h (Fig. 2d). In addition to the evolution of morphology, for the film sintered at 1223 K, it seems that the $\text{Ca}_3\text{Co}_4\text{O}_{9+\delta}$ grains began to be sintered together forming a connective structure (Fig. 2d). The thickness of the film after sintering at 1223 K for 2 h was determined by SEM to be about 60 μm .

Figure 3a-d displays the SEM images taken from the fracture cross-sections of $\text{Ca}_{3-x}\text{Ag}_x\text{Co}_4\text{O}_{9+\delta}$ thick-films, which were sintered at 1223 K for 2 h in air, with $x = 0, 0.05, 0.10$, and 0.15 , respectively. Although all investigated films exhibit a similar porous structure these films show some lamella-like grains, particularly the grains at the region close to the substrate surface. This lamella-like morphology looks more pronounced for the films containing Ag (Fig. 3b-d) than the one with pure $\text{Ca}_3\text{Co}_4\text{O}_{9+\delta}$ (Fig. 3a).

In order to determine porosity of the sintered-films, SEM images from the polished cross-section were performed for all the investigated samples, and shown in figure 4 is a SEM image of a typical $\text{Ca}_{2.95}\text{Ag}_{0.05}\text{Co}_4\text{O}_{9+\delta}$ thick-film. The porosity was determined to be about 43% using “Simple Phase Analyzer” software to analyze the images by counting the black and grey pixels. There was no significant difference in porosity between the samples, indicating that all the thick-films show a similar porous structure.

Temperature dependence of the electrical resistivity for thick-films $\text{Ca}_{3-x}\text{Ag}_x\text{Co}_3\text{O}_{9+\delta}$ with $x = 0, 0.05, 0.10$, and 0.15 , sintered at 1223 K for 2 h in air are shown in figure 5. The data of the cold-isostatic-pressed (CIP) pure $\text{Ca}_3\text{Co}_4\text{O}_{9+\delta}$ sample is also presented for comparison. Overall, the electrical resistivity of thick-film is comparable and slightly lower than that of the CIP-sample. Thick-film of pure $\text{Ca}_3\text{Co}_4\text{O}_{9+\delta}$ sample exhibited a higher electrical resistivity, probably due to the porous structure of the film as compared with the CIP-sample, which has a relative density about

76% of the theoretical density (i.e. a porosity of ~24%). It is clearly shown from Fig. 5 that the electrical resistivity of all investigated samples exhibited opposite behavior in two temperature regions $T < 600$ K and $T > 600$ K. The resistivity of the samples below about 600 K tended to decrease with increasing temperature, while above 600 K the resistivity of the samples increased rapidly. This phenomenon could be related to the oxygen deficiency. At high temperatures (i.e. above 600 K), oxygen is probably released due to the porous structure under a low pressure of helium atmosphere. In the $\text{Ca}_3\text{Co}_4\text{O}_{9+\delta}$ system, the majority of the charge carriers are hole-type, as confirmed by the positive values of the Seebeck and Hall coefficients.¹³ Three types of valences of Co ions: Co^{2+} , Co^{3+} , and Co^{4+} are supposed to exist in this system, and the concentration of Co^{4+} is responsible for the hole concentration.¹⁵ Taking the following formula into account $\text{Ca}_3^{+2}\text{Co}_4^{+\nu}\text{O}_{9+\delta}^{-2}$, due to charge neutrality the sum of valences of all compounds must be equal zero therefore should fulfill the following condition,

$$\nu = \frac{\delta + 6}{2} \quad (1)$$

where ν is the average valence of Co. From formula (1), one can see that the average valence of Co will decrease if δ is decreased, particularly when $\delta < 0$. The decrease in the average Co valence results in the decrease in the Co^{4+} content i.e. the hole concentration, and thus decrease the electrical conductivity of the system. Since all samples were measured in vacuum with the presence of small amount of helium gas, the oxygen release is progressively increasing with increasing the temperature and thereby affects the hole Co^{4+} concentration, and the stability of $\text{Ca}_3\text{Co}_4\text{O}_{9+\delta}$ phase. It was also found in a complex cobalt oxide $\text{Sr}_{0.7}\text{Y}_{0.3}\text{CoO}_{2.62}$ that the oxygen content starts decreasing rapidly in helium at a temperature of ~100 degrees lower than in air¹⁷. As for $\text{Ca}_3\text{Co}_4\text{O}_{9+\delta}$ system, the loss of oxygen ion was observed to start at about 723 K¹⁸ in air. Moreover even under the condition where the $\text{Ca}_3\text{Co}_4\text{O}_{9+\delta}$ is still stable, the oxygen content systematically decreased with increasing temperature and decreasing oxygen pressure, as confirmed in the work¹⁶ by Shimoyama *et al.*. Notably, all the samples with Ag addition showed a lower value of electrical resistivity than the pure $\text{Ca}_3\text{Co}_4\text{O}_{9+\delta}$ sample at temperatures below 600 K.

Figure 6 shows the Seebeck coefficient (S) as a function of temperature for all samples. In general, the Seebeck coefficient of all investigated samples increases with increasing temperature, and the S values are positive over the whole measured temperature range, indicating p -type

semiconducting materials. At temperatures below 600 K, S gradually increased, while it suddenly raised when the temperature is increased over 600 K. The rapidly increase of S in the temperature region above 600 K could be associated with the abruptly decrease in the hole concentration due to the oxygen deficiency at high temperatures aforementioned. Interestingly, among all investigated samples the $\text{Ca}_{3-x}\text{Ag}_x\text{Co}_3\text{O}_{9+\delta}$ with $x = 0.05$ thick-film showed the highest Seebeck coefficient over the whole measured temperature range. The enhanced Seebeck coefficient might be related to the formation of a fine-scale distribution of metallic Ag as nanoinclusions, the detailed microstructure of these films using HRTEM, STEM-EDX will be carried out in the future to identify the size and the distribution of these particles. The interfaces between the metallic nanoinclusion (Ag) and the semiconductor host (cobaltite) probably play a role both in blocking phonon transport and in favoring charge-carrier transport as observed in bulk samples.⁹ Theoretical calculations indicated that for any size of nanoinclusions the Seebeck coefficient always becomes larger than that of the inclusion-free system.¹⁹ This enhancement was explained by the strongly energy dependent scattering time of electrons at the interface between metallic inclusion and the semiconducting host matrix. However, for a higher Ag concentration, e.g. the sample at $x = 0.15$, the high Ag content could lead to the percolation or agglomeration of Ag particles causing a high electrical conductivity but also lowering the Seebeck coefficient by short-circuiting the thermoelectric voltage within the cobaltite grains.²⁰ The observation of the enhanced Seebeck coefficient on the thick-film with $x = 0.05$ is in good agreement with the reported bulk nanostructured misfit-layered cobaltite on the same Ag concentration⁹ and indicate the existence of fine Ag particles.

Power factor (S^2/ρ) of the thick-films $\text{Ca}_{3-x}\text{Ag}_x\text{Co}_3\text{O}_{9+\delta}$ with $x = 0, 0.05, 0.10$, and 0.15 as well as the CIP-sample as a function of temperature is presented in figure 7. The maximum power factor were found at 612 K to be 0.18, 0.3, 0.19, and 0.23 mW/mK² for the samples $x = 0, 0.05, 0.10, 0.15$, respectively. It is clear from Fig. 7 that the highest measured power factor is belong to the $x = 0.05$ thick-film, showing a value of about 67% higher than the film of pure $\text{Ca}_3\text{Co}_4\text{O}_{9+\delta}$.

CONCLUSIONS

In summary, we have investigated the high temperature thermoelectric properties and microstructure of a series of $\text{Ca}_{3-x}\text{Ag}_x\text{Co}_3\text{O}_{9+\delta}$ thick-films for $0 \leq x \leq 0.15$, which were prepared by a simple and low cost process – screen printing. The observations of the microstructure indicated

that the films sintered at 1223 K for 2 h in air have porous structure with “plate-like” and “lamella-like” grains morphology. At temperatures below 612 K, the power factor was improved for the samples with Ag addition mainly due to the reduction of the electrical resistivity. Strikingly, power factor for the $x = 0.05$ film attained at 612 K a maximum power factor value of $\sim 0.3 \text{ mW/mK}^2$, which is about 67% higher than the film of pure $\text{Ca}_3\text{Co}_4\text{O}_{9+\delta}$. This initial observation is promising for further investigations such as the thermal conductivity measurements to determine the figure-of-merit, and the improvement of ZT through optimizing material composition.

ACKNOWLEDGEMENTS

The authors would like to thank the Programme Commission for Energy and Environment (EMNi), The Danish Research and Innovations (Project # 10-093971) for sponsoring the OTE-POWER research work.

REFERENCES

1. J. Karni, *Nat. Mater.* 10, 481 (2011). doi:[10.1038/nmat3057](https://doi.org/10.1038/nmat3057).
2. Y. Pei, X. Shi, A. LaLonde, H. Wang, L. Chen and G.J. Snyder, *Nature*. 473, 66 (2011). doi:[10.1038/nature09996](https://doi.org/10.1038/nature09996).
3. D. Kraemer, B. Poudel, H-P. Feng, J.C. Caylor, B. Yu, X. Yan, Y. Ma, X. Wang, D. Wang, A. Muto, K. McEnaney, M. Chiesa, Z. Ren and G. Chen, *Nat. Mater.* 10 [7], 532 (2011). doi:[10.1038/nmat3013](https://doi.org/10.1038/nmat3013).
4. T. Ohta, T. Kajikawa and Y. Kumashiro, *Electr. Eng. Jpn.* 110 [4], 14 (1990). doi:[10.1002/eej.4391100402](https://doi.org/10.1002/eej.4391100402).
5. H.B. Lee, H.J. Yang, J.H. We, K. Kim, K.C. Choi and B.J. Cho, *J. Electron. Mater.* 40 [5], 615 (2011).
6. H.B. Lee, J.H. We, H.J. Yang, K. Kim, K.C. Choi and B.J. Cho, *Thin Solid Films* 519, 5441 (2011). doi:[10.1016/j.tsf.2011.03.031](https://doi.org/10.1016/j.tsf.2011.03.031).
7. G. D. Tang, H.H. Guo, T. Yang, D.W. Zhang, X.N. Xu, L.Y. Wang, Z.H. Wang, H.H. Wen, Z.D. Zhang and Y.W. Du, *Appl. Phys. Lett.* 98, 202109 (2011). doi:[10.1063/1.3592831](https://doi.org/10.1063/1.3592831).
8. K. Ahmad and A. Lowe, *J. Am. Ceram. Soc.* 94 [2] 611 (2011). doi:[10.1111/j.1551-2916.2010.04106.x](https://doi.org/10.1111/j.1551-2916.2010.04106.x).
9. N. V. Nong, N. Pryds, S. Linderöth and M. Ohtaki, *Adv. Mater.* 23 [21], 2484 (2011). doi:[10.1002/adma.201004782](https://doi.org/10.1002/adma.201004782).
10. N. V. Nong, S. Yanagiya, S. Monica, N. Pryds and M. Ohtaki, *J. Electron. Mater.* 40 [5], 716 (2011). doi:[10.1007/s11664-011-1524-1](https://doi.org/10.1007/s11664-011-1524-1).
11. N. V. Nong, C. J. Liu and M. Ohtaki, *J. Alloys Compd.* 509, 977 (2011). doi:[10.1016/j.jallcom.2010.09.150](https://doi.org/10.1016/j.jallcom.2010.09.150).
12. C.J. Liu, Y.C. Huang, N. V. Nong, Y.L. Liu and V. Petříček, *J. Electron. Mater.* 40 [5], 1042 (2011). doi:[10.1007/s11664-011-1527-y](https://doi.org/10.1007/s11664-011-1527-y).
13. N.V. Nong, C-J. Liu and M. Ohtaki, *J. Alloys Compd.* 491, 53 (2010). doi:[10.1016/j.jallcom.2009.11.009](https://doi.org/10.1016/j.jallcom.2009.11.009).
14. Y. Wang, Y. Sui, J. Cheng, X. Wang, W. Su, *J. Alloys Compd.* 477, 817 (2009). doi:[10.1016/j.jallcom.2008.10.162](https://doi.org/10.1016/j.jallcom.2008.10.162).
15. D. Wang, L. Cheng, Q. Yao and J. Li, *Solid State Comm.* 129, 615 (2004). doi:[10.1016/j.ssc.2003.11.045](https://doi.org/10.1016/j.ssc.2003.11.045).

16. J. Shimoyama, S. Horii, K. Otzchi, M. Sano and K. Kishio, *Jpn. J. Appl. Phys.* 42, L194 (2003). doi:10.1143/JJAP.42.L194.
17. S.Ya. Istomin, J. Grins, G.Svensson, O.A. Drozhzhin, V.L. Kozhevnikov, E.V. Antipov and J.P. Attfield, *Chem. Mater.* 15, 4012 (2003). doi:10.1021/cm034263e.
18. J.D. Zhou, L.R. Pederson, E. Thomsen, Z. Nie and G. Coffey, *Electrochem. Solid-State Lett.* 12 [2], F1 (2009). doi:10.1149/1.3039948.
19. S.V. Faleev, F. Leonard, *Phys. Rev. B* 77, 214304 (2008). doi:10.1103/PhysRevB.77.214304.
20. M. Mikami, N. Ando, R. Funahashi, *J. Solid State Chem.* 178, 2186 (2005). doi:10.1016/j.jssc.2005.04.027.

FIGURE CAPTIONS

Fig. 1. X-ray powder diffraction patterns at room temperature for $\text{Ca}_{3-x}\text{Ag}_x\text{Co}_3\text{O}_{9+\delta}$ with $x = 0, 0.05, 0.10$, and 0.15 after calcining at 1223 K for 24 h in air.

Fig. 2. SEM images of the fractured surfaces of pure $\text{Ca}_3\text{Co}_4\text{O}_{9+\delta}$ thick-film, as sintered in air at 973 K for 1 h (a), 1123 K for 1 h (b), 1173 K for 2 h (c), and 1223 K for 2 h (d).

Fig. 3. SEM images of the fractured surfaces of $\text{Ca}_{3-x}\text{Ag}_x\text{Co}_3\text{O}_{9+\delta}$ thick-films after sintering at 1223 K for 2 h in air: (a) is for $x = 0$, (b) for $x = 0.05$, (c) for $x = 0.10$, and (d) for $x = 0.15$.

Fig. 4. SEM image of the polished cross-section of a typical $\text{Ca}_{2.95}\text{Ag}_{0.05}\text{Co}_4\text{O}_{9+\delta}$ thick-film.

Fig. 5. Temperature dependence of the electrical conductivity for $\text{Ca}_{3-x}\text{Ag}_x\text{Co}_3\text{O}_{9+\delta}$ thick-films with $x = 0, 0.05, 0.10$, and 0.15 after sintering at 1223 K for 2 h in air, and the CIP-sample after sintering under the same conditions for 24 h .

Fig. 6. Temperature dependence of the Seebeck coefficient for $\text{Ca}_{3-x}\text{Ag}_x\text{Co}_3\text{O}_{9+\delta}$ thick-films with $x = 0, 0.05, 0.10$, and 0.15 and the CIP-sample.

Fig. 7. Temperature dependence of the power factor for $\text{Ca}_{3-x}\text{Ag}_x\text{Co}_3\text{O}_{9+\delta}$ thick-films with $x = 0, 0.05, 0.10$, and 0.15 and the CIP-sample.

Figure 1
[Common.Links.ClickHereToDownloadHighResolutionImage](#)

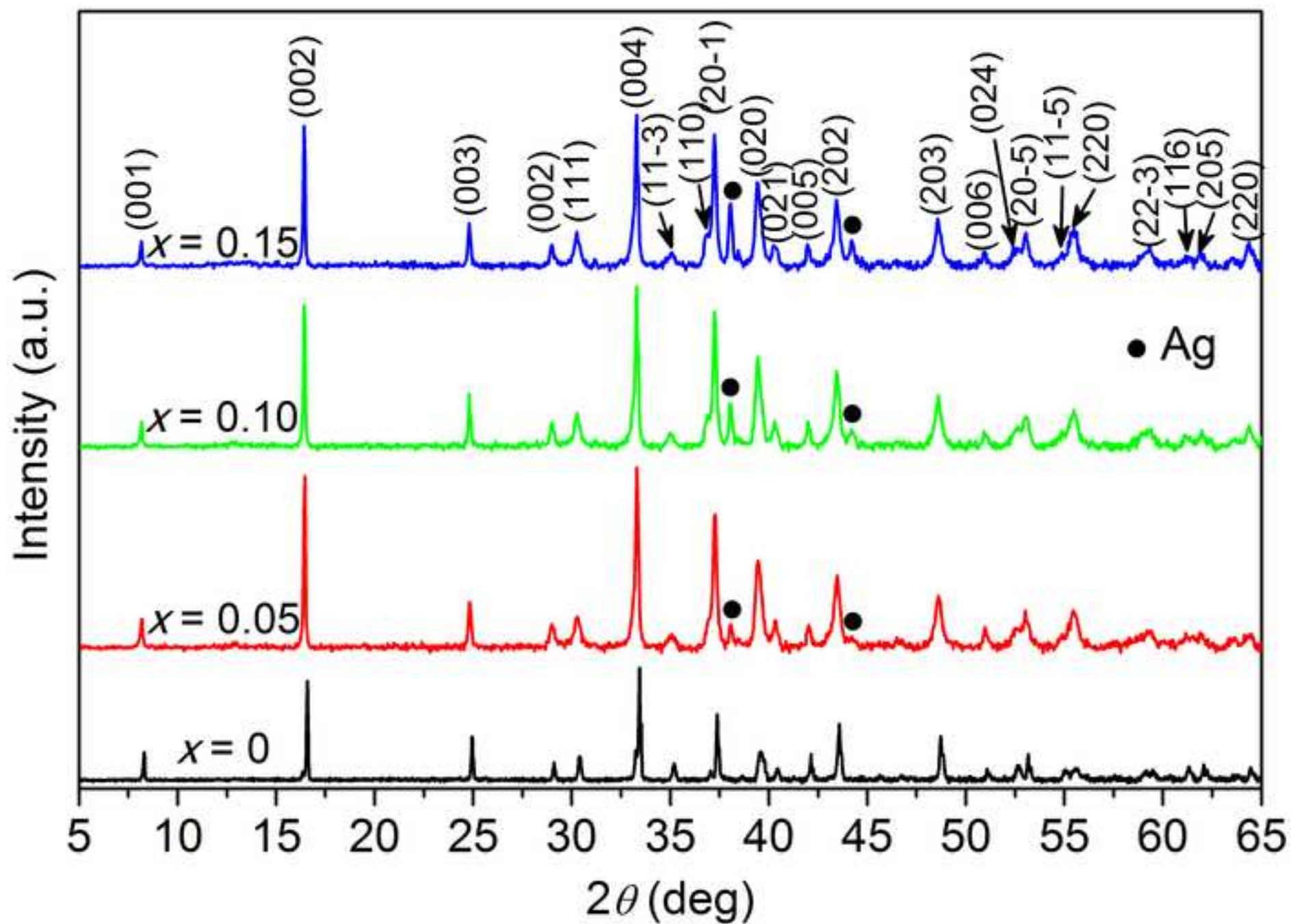


Figure 2
[Common.Links.ClickHereToDownloadHighResolutionImage](#)

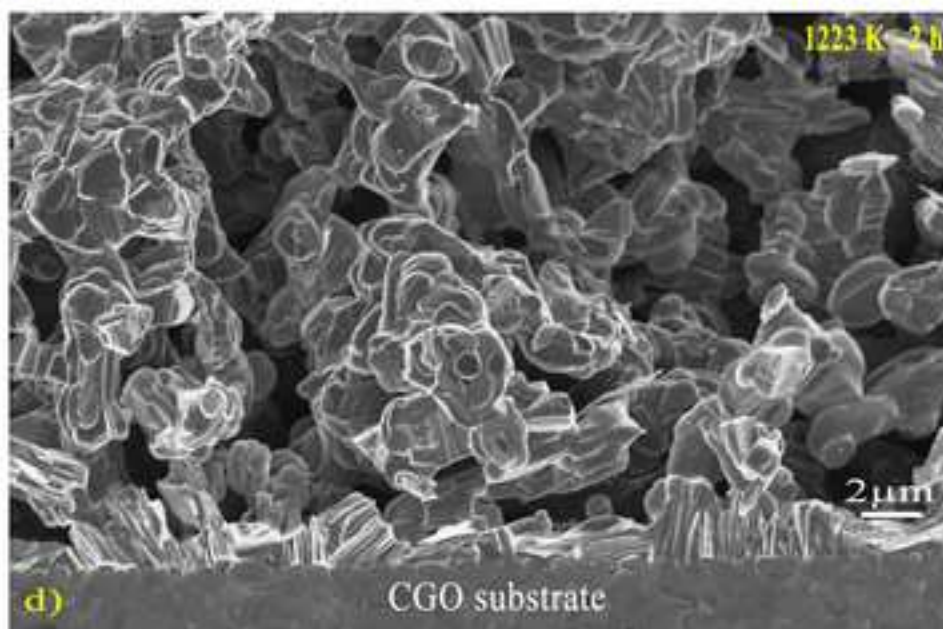
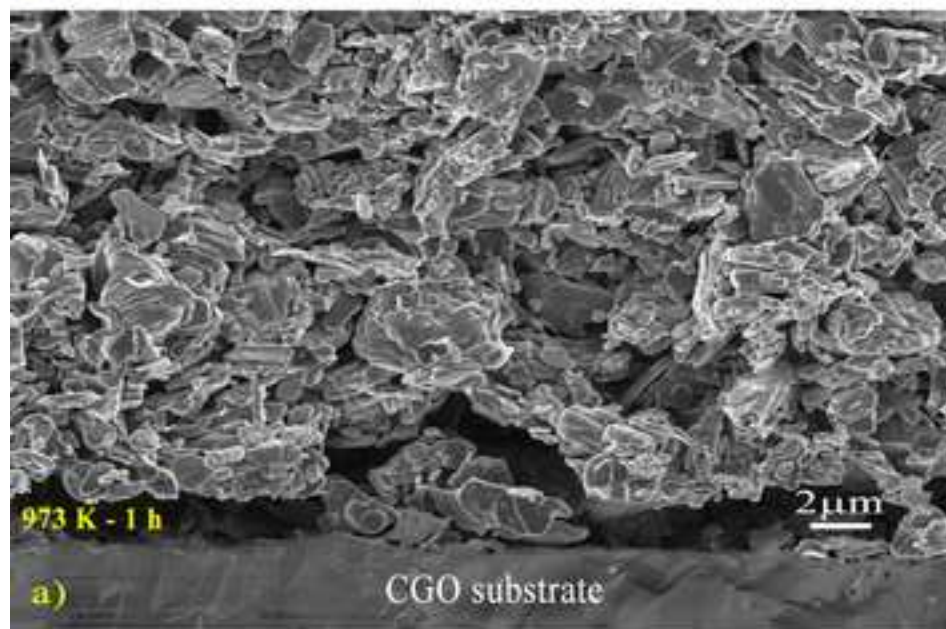
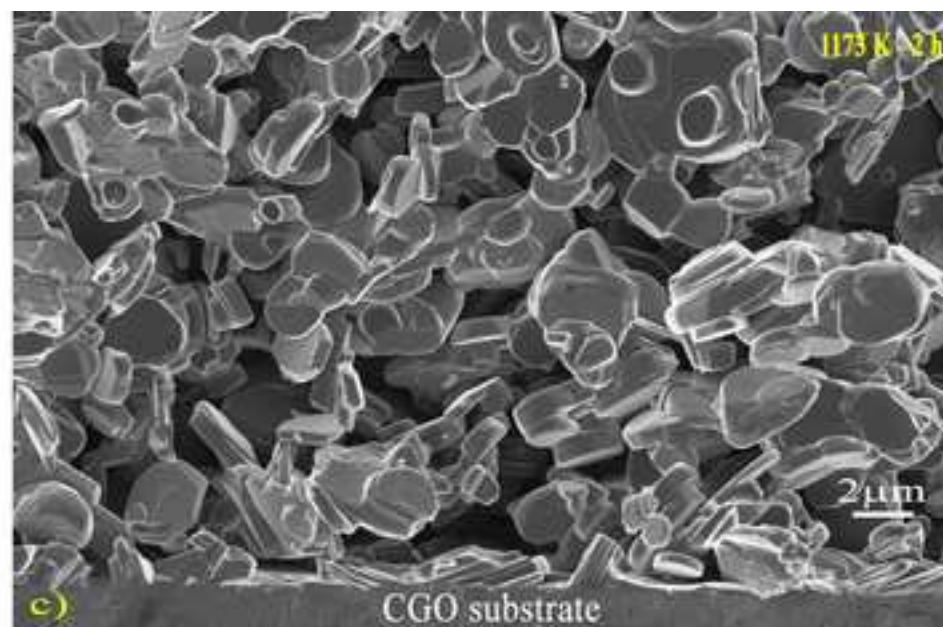
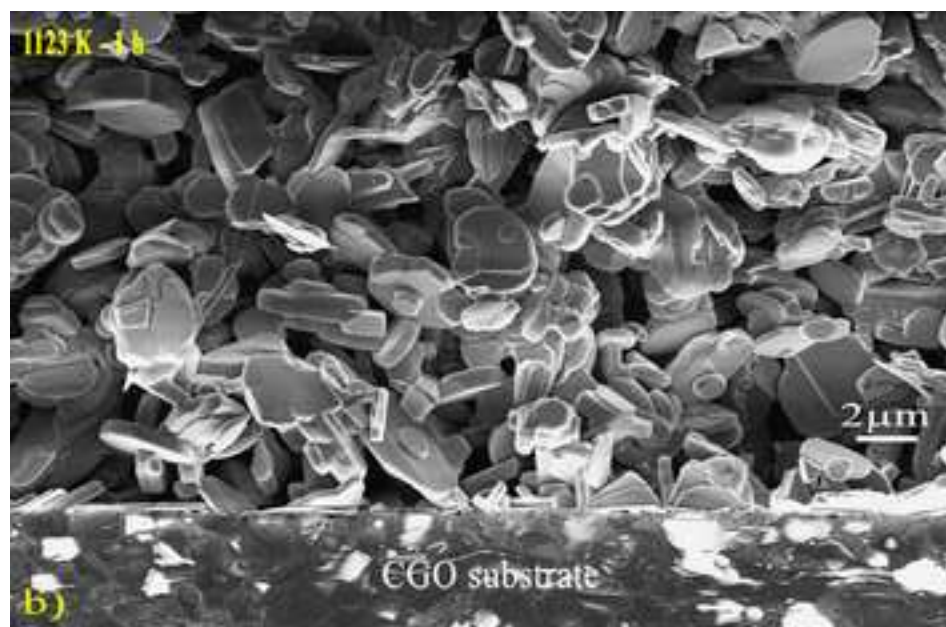


Figure 3
[Common.Links.ClickHereToDownloadHighResolutionImage](#)

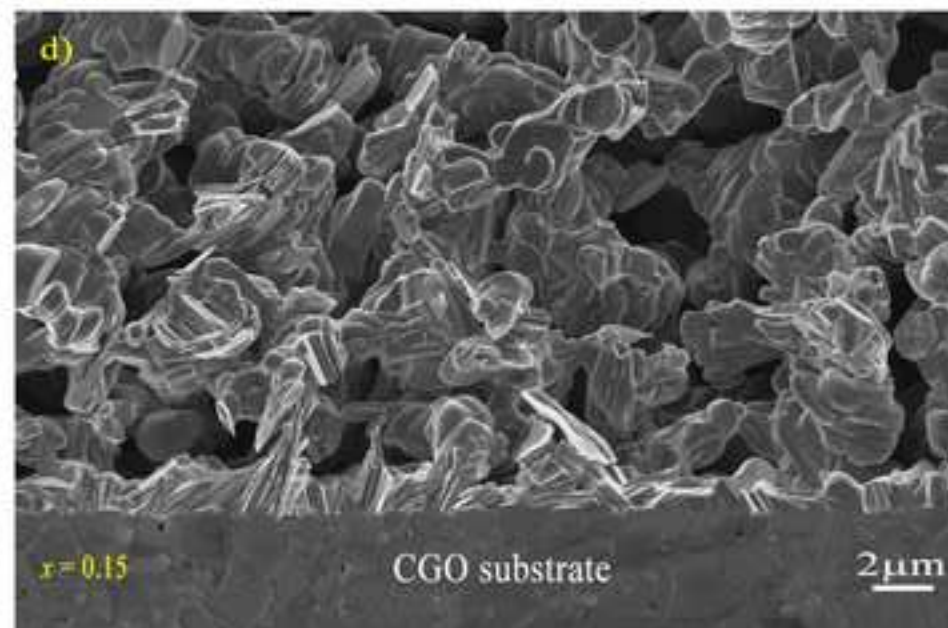
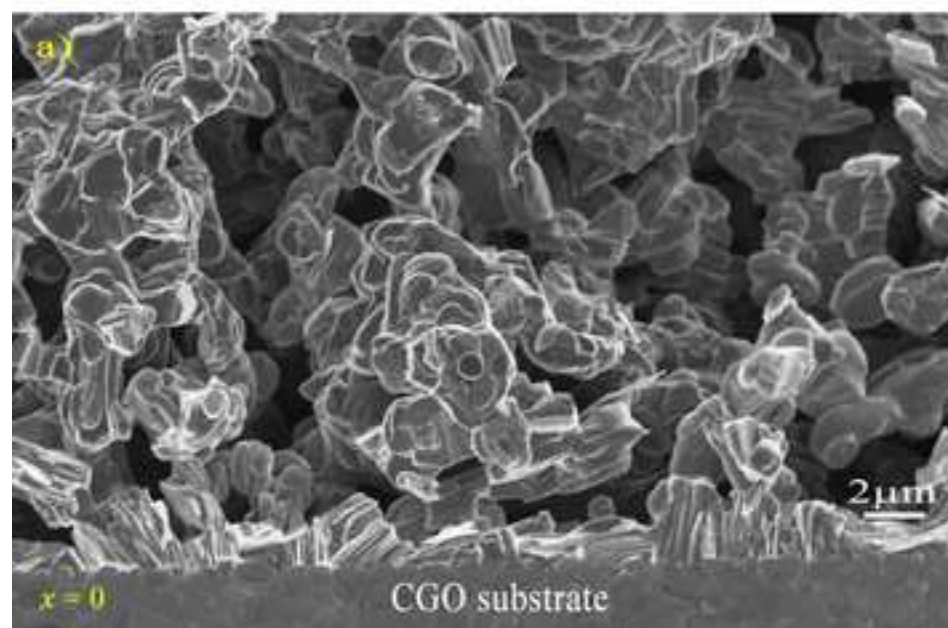
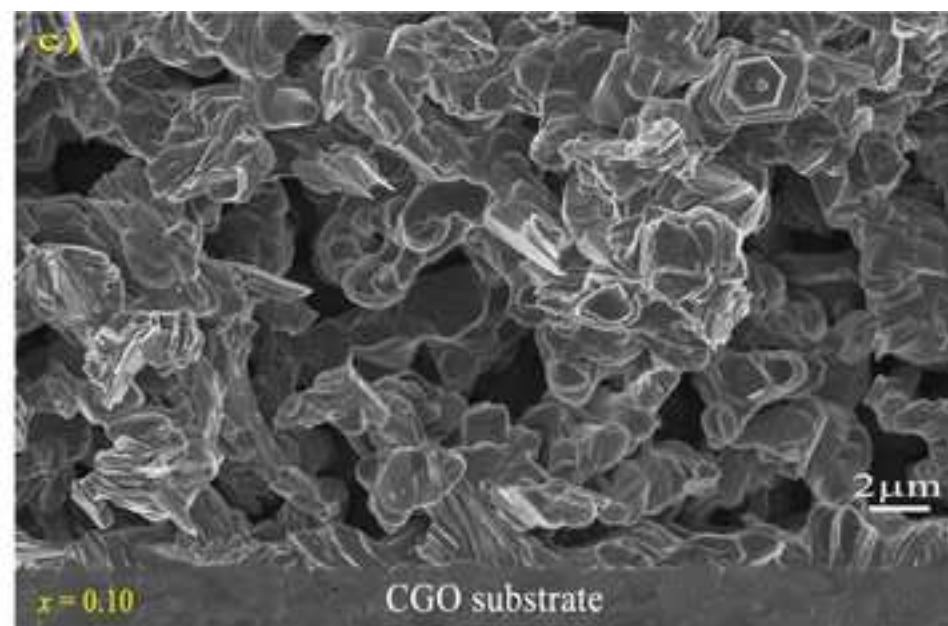
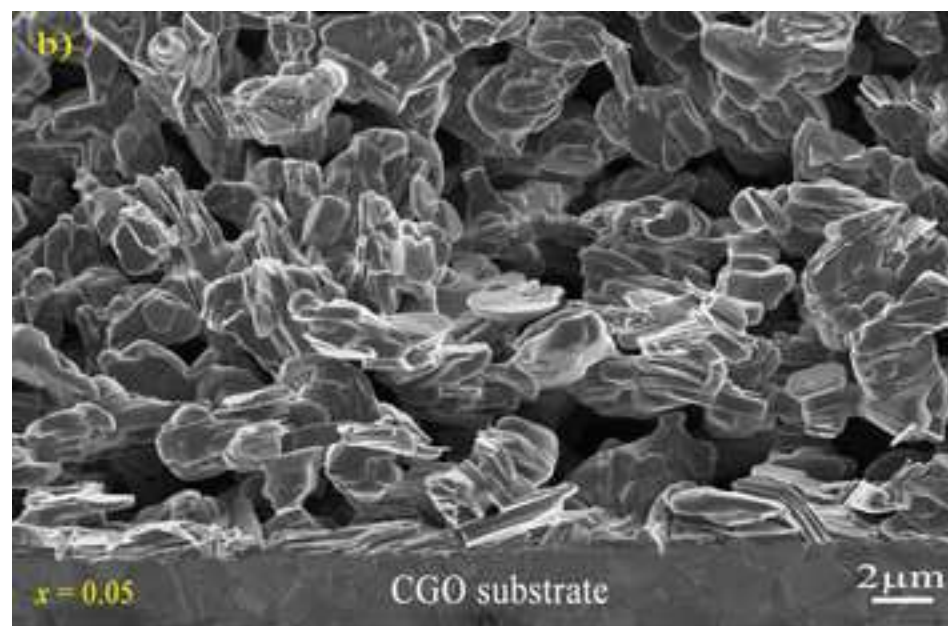


Figure 4

[Common.Links.ClickHereToDownloadHighResolutionImage](#)

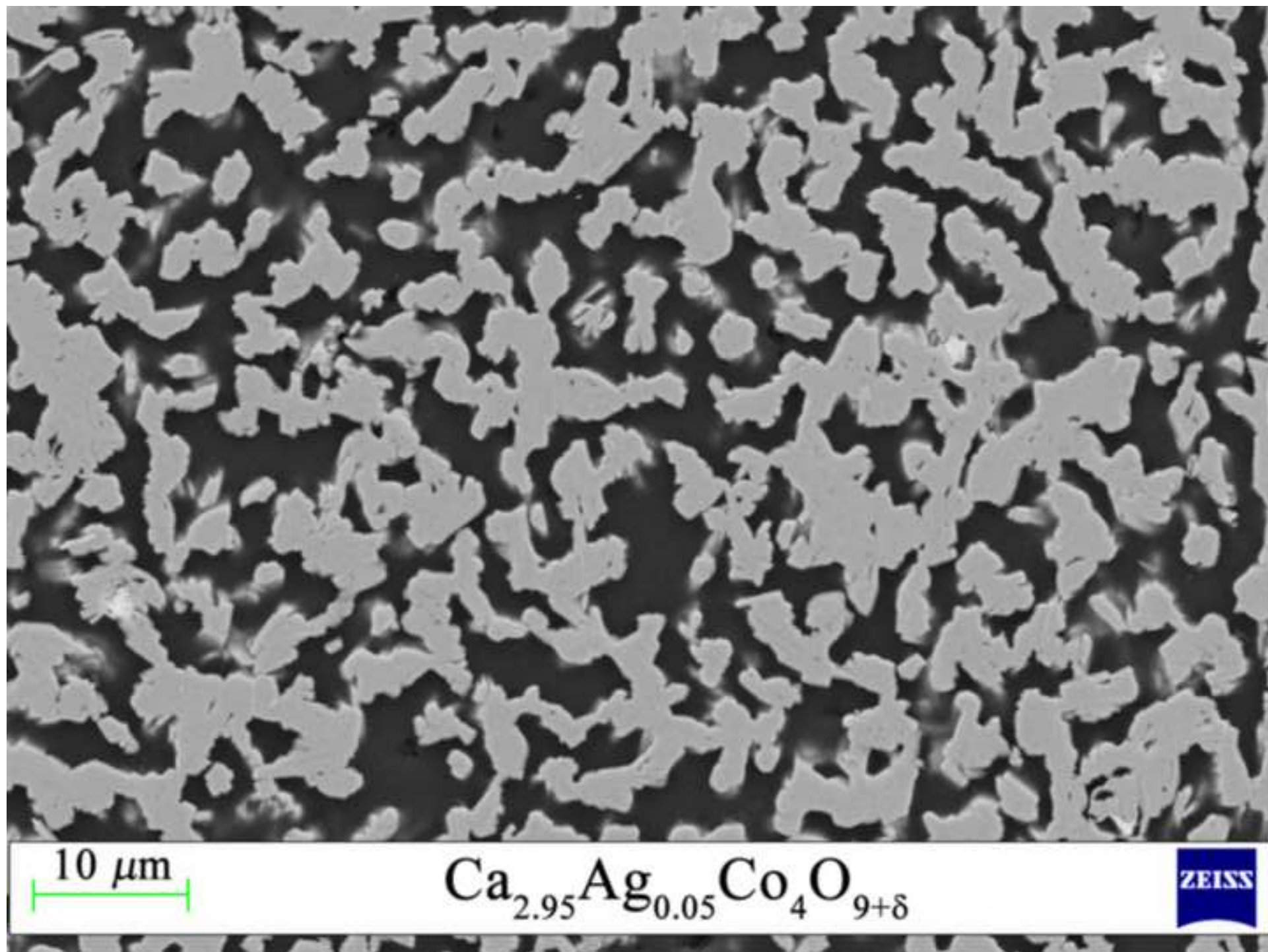


Figure 5

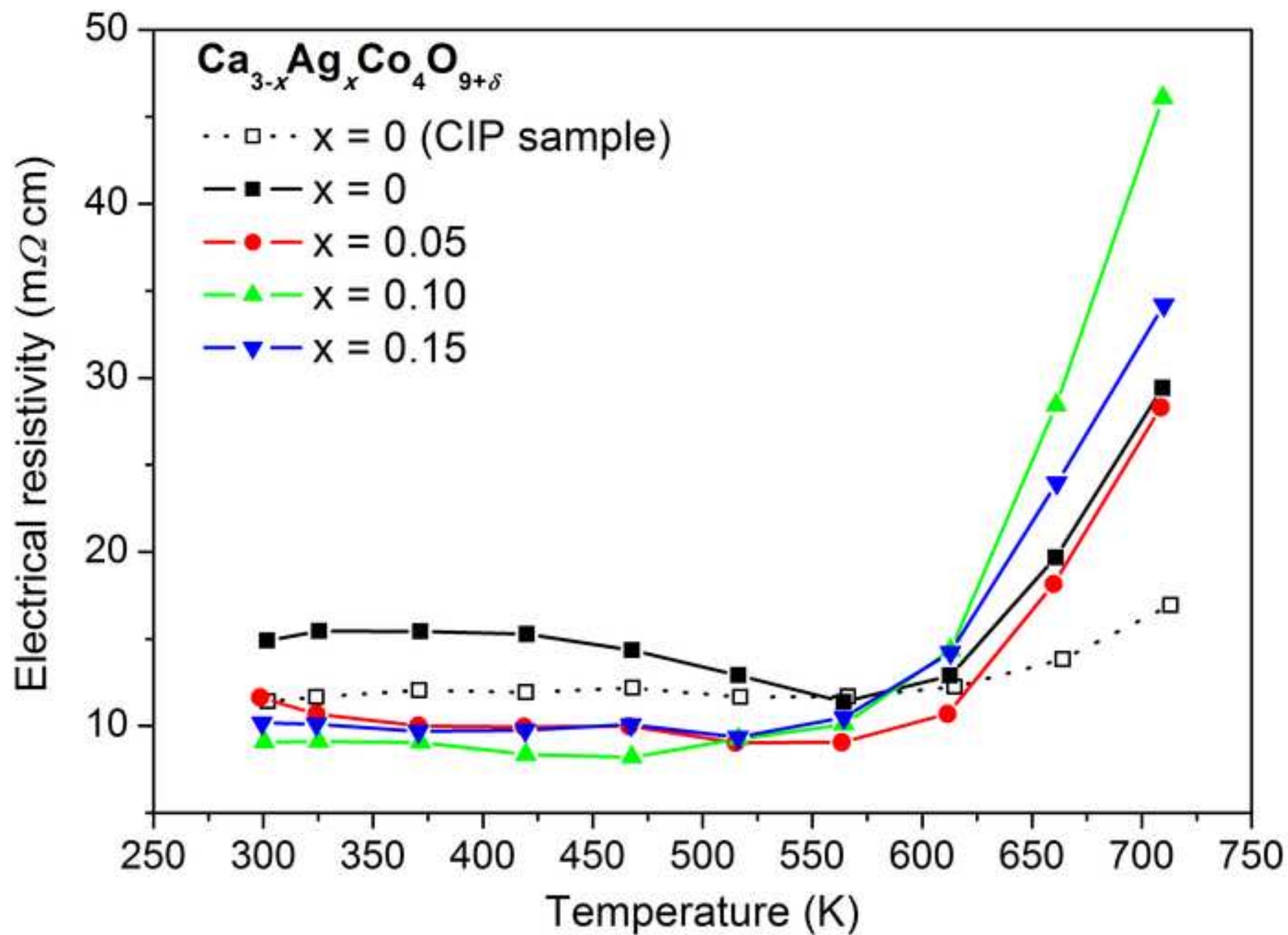
[Common.Links.ClickHereToDownloadHighResolutionImage](#)

Figure 6
[Common.Links.ClickHereToDownloadHighResolutionImage](#)

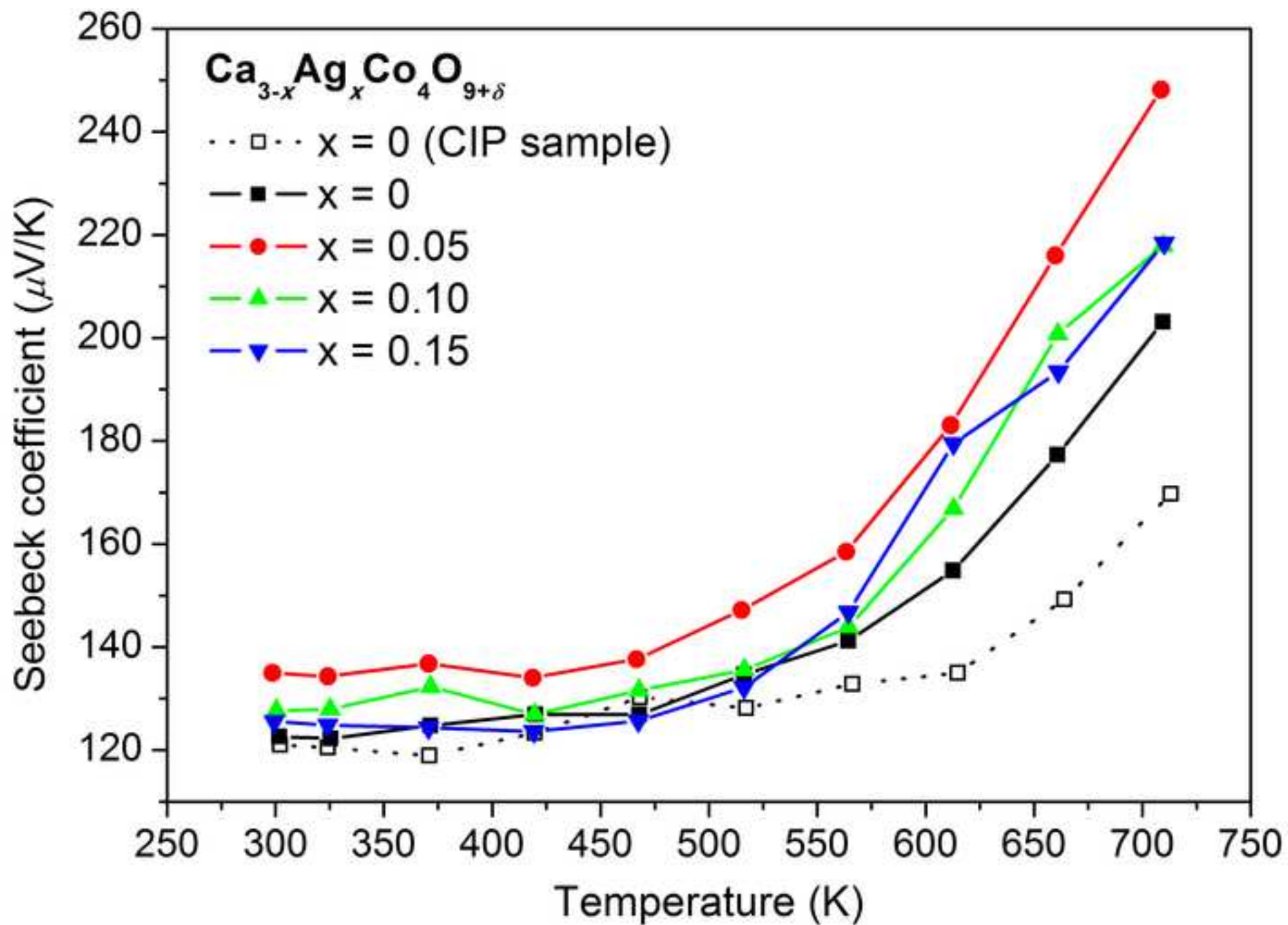


Figure 7

[Common.Links.ClickHereToDownloadHighResolutionImage](#)